NANO LETTERS

2008
Vol. 8, No. 1
345−349

Formation and Self-Breaking Mechanism of Stable Atom-Sized Junctions

Makusu Tsutsui,[†] Kohei Shoji,[†] Masateru Taniguchi,*[,†,‡] and Tomoji Kawai[†]

The Institute of Scientific and Industrial Research, Osaka University, Ibaraki, Osaka 567-0047, Japan, and PRESTO, Japan Science and Technology Agency, Honcho, Kawaguchi, Saitama 332-0012, Japan

Received November 17, 2007

ABSTRACT

The self-breaking mechanism of gold junctions is studied by investigating stability of the atom-sized contacts. The single atom contact lifetime increases from about 0.02 to 200 s upon decreasing the junction stretching speed, while at the same time, the breaking force diminishes logarithmically. We find that the junction self-breaking processes involve sufficient atomic rearrangements, which thereby allow complete self-compensation of externally introduced strain at 0.8 pm/s. The present results have important implications on fabrication of stable single molecule junctions.

The fabrication of reliable nanometer-spaced electrodes is a first step toward the realization of single molecule electronics. Various techniques have been developed to form stable metal/molecule/metal junctions and extensively applied for studying electron transport in single molecules.[1−5] The electromigration-induced break junction is one of the most promising techniques from practical perspectives: the compatiblity with standard silicon microfabrication techniques and the accompanying facility to incorporate gate electrodes.[5,6] However, attaining precise control of the gap size has proved to be challenging; during the active breaking process, mutual effects of electromigration and bias-induced local heating trigger melting and surface tension.[7,8] As a result, the gap distance unintentionally becomes large and metal nanoparticles are occasionally generated in the gap region, the electrical characteristics of which mimic that of single molecules.[6,8−10]

The self-breaking scheme has been demonstrated to be effective for suppressing possible nanoparticle formation.[11,12] In this method, a Au junction is first narrowed to atomic size by active breaking through electromigration. Subsequently, the atom-sized junctions are subjected to undergo spontaneous breaking under null electric field. As a consequence, particle-free nanogap electrodes can be obtained with high yield. Nevertheless, the success rates of molecular trapping in the self-breaking method are so far moderate.[11,12] In an effort to refine the technique, therefore, it is of practical importance to investigate the underlying physics of the self-breaking mechanism of the nanojunctions.

The mechanically controllable break junction (MCBJ) is expected to be a practical test bed for this purpose, since junction breaking can be implemented repeatedly for hundreds of times on one sample. Particularly, lithographically defined MCBJs enable fine-tuning of junction displacement with subpicometer resolution,[13−15] a requisite for conducting reliable measurements on the junction self-breaking characteristics. In the present study, the nanofabricated MCBJs are exploited to explore the self-breakdown mechanism of atom-sized junctions at room temperature by evaluating the stability of single atom contacts under various displacement rate conditions down to 0.8 pm/s.

The principle of operations and technical details of the nanofabricated MCBJ are described elsewhere.[13,14] A polished phosphor bronze substrate of thickness $t = 0.5$ mm is spin-coated with a polyimide layer for electrical insulation. Nanoscale Au junctions with a typical dimension of 100 nm × 100 nm (width × thickness) are patterned on the polyimide-coated substrate exploiting a standard electron-beam lithography and a lift-off technique. Metal deposition (Au/Cr = 100 nm/1 nm) is exhibited by means of radio frequency magnetron sputtering. Subsequently, the polyimide underneath the junctions is removed by isotropic reactive ion etching using O_2/CF_4 plasma, and a free-standing Au nanobridge of length $u \sim 4$ μm is obtained. Finally, the sample is annealed at 250 °C to eliminate possible structural disorders contained in the junctions. A scanning electron microscopy image of a typical contact configuration is shown in Figure 1a. The sample is mounted in a three-point bending mechanism, which is then bent mechanically with a piezo-actuator backed by a screw-driven mechanism. As a result, the junction is stretched and eventually broken. A reduction factor r, defined as a ratio between the elongation of the

* Corresponding author. Tel: +81-6-6879-4289. Fax: +81-6-6879-4289. E-mail: tanigu32@sanken.osaka-u.ac.jp.
[†] Osaka University.
[‡] Japan Science and Technology Agency.

10.1021/nl073003j CCC: $40.75
Published on Web 12/21/2007

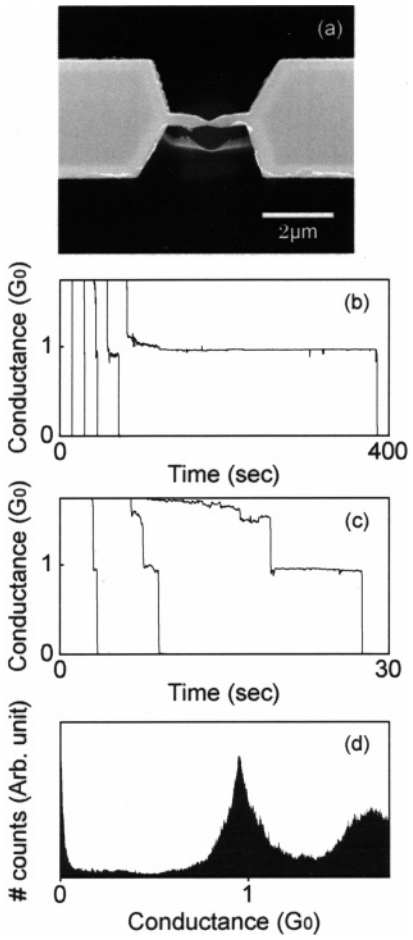

Figure 1. (a) Scanning electron micrograph of a typical nanoMCBJ configuration. (b) Temporal conductance curve during breaking of Au atom-sized contacts at various displacement rates v_d (8, 0.8, 0.08, 0.008, and 0.0008 nm/s from left). (c) Expanded description of the three conductance traces at the left in panle a. (d) A typical conductance histogram constructed from 1000 traces showing a prominent $1G_0$ peak.

junction, Δd, and the translation of the pushing rod, Δz, is $r = \Delta d/\Delta z = 6ut/L^2 \sim 3 \times 10^{-4}$ with our experimental set up, where L is a distance between the countersupports. The small r enables fine control of the contact breaking with subpicometer resolution.

The contact forming and breaking conditions are controlled by an automated feedback program. Junction closing is performed at a displacement rate of $v_d = 0.8$ nm/s until the contact conductance G increases to $G > 10G_0$, where $G_0 = 2e^2/h$ is the conductance quantum. Subsequently, the junction is opened initially at $v_d = 4$ nm/s. When the contact is stretched to below $10G_0$, the displacement speed is slowed to $v_d = 0.4$ nm/s. When it is further thinned to $G \sim 5G_0$, breaking of the contact is launched, which is undertaken at various v_d's from 8 to 0.0008 nm/s. Temporal conductance change during the contact breaking is measured. The contact conductance states are tracked continuously by using a picoammeter. Simultaneously, a fast digital oscilloscope is utilized to capture rapid fracture processes. All measurements are performed under a constant bias of 0.1 V at room temperature in vacuum.

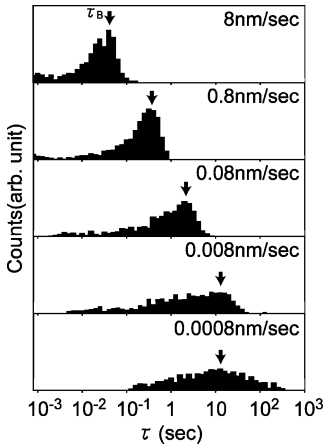

Figure 2. Single atom contact lifetime distributions obtained at various v_d's. The lifetime is taken in a logarithmic scale. Each $P(\tau)$ represents a single peak profile. The peak life time τ_B, indicated by black arrows, monotonically shifts to high-τ range with decreasing v_d.

Typical conductance curves during contact breaking at various v_d conditions are displayed in Figure 1, panels b and c. The well-defined $1G_0$ plateaus signify formation of Au single atom contacts (SACs). Accordingly, a sharp peak appears at $1G_0$ in the conductance histogram constructed from 1000 traces (Figure 1c). Influence of the displacement rates is reflected in the orders of magnitude difference in the $1G_0$ plateau length, which denotes the life time τ of the SACs. τ is defined as the amount of time that the contact conductance stays within $0.8G_0$ to $1.2G_0$. For the traces in Figure 1, for example, $\tau \sim 0.1$ and ~ 200 s for $v_d = 8$ and 0.0008 nm/s, respectively. However, the contact lifetime shows vast variation even under an identical experimental condition. Single atom contacts are predicted to undergo a thermally activated fracture at room temperature, and the lifetime is theoretically described by the Arrhenius form as

$$\tau = \tau_0 \exp[(E_B - \zeta V - \alpha F)/k_B T_{eff}] \quad (1)$$

$$T_{eff}^4 = T_0^4 + T_V^4 \quad (2)$$

where E_B and T_{eff} denote the energy barrier for breaking contacts and contact effective temperature.[16,17] The effective energy barrier decreases by the external tensile forces, αF, and the current-induced forces, ζV. Local ionic heating also contributes to contact destabilization through $T_V = \Gamma(LV)^{1/2}$, where L is the effective chain length and Γ is a material dependent parameter.[16] Note that τ is exponentially dependent on E_B. This E_B is determined by atomic arrangements of the contacts. Since it is not possible to exactly control contact deformations and reproduce an identical atomic arrangements, the expansive diversity in τ is naturally interpreted as indicating the unavoidable difference in the contact geometries.

In order to examine effects of stretching rate on the contact breakdown mechanism, therefore, τ is corrected for 1000 traces obtained at each v_d condition and analyzed statistically. The $1G_0$ plateau length distribution, $P(\tau)$, obtained at

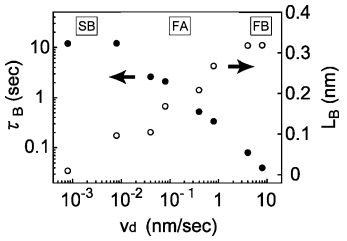

Figure 3. Semilogarithmic plot of the contact breaking length versus the stretching rate, which explicitly shows three distinct realms: the force-breaking regime, the force-accelerated spontaneous breakdown regime, and the self-breaking regime.

different stretching rates is depicted in Figure 2. The $P(\tau)$ reveals wide variations in τ that span over more than 2 orders of magnitude, representing aforementioned irreproducibility of the contact configurations (note that τ is taken in a logarithmic scale). Interestingly, however, $P(\tau)$ at each υ_d shares a similar single peak structure. It is expected that sufficient contact structure relaxation occurs during mechanical elongation under low stretching rate conditions considering gold atoms are relatively mobile at a room temperature. As a result, stable contacts of a particular configuration are statistically favored to form, giving rise to a narrow distribution of E_B and, hence, the single peak $P(\tau)$ profile.[18] We extracted the peak life time τ_B of $P(\tau)$. The characteristic contact breaking length L_B is calculated from τ_B by $L_B = \upsilon_d\tau_B$ assuming the contacts are elongated at a uniform rate υ_d, and plotted as a function of υ_d along with τ_B in Figure 3. The (τ_B, L_B) − υ_d plots reveal three distinct regions: the force-breaking (FB) regime, where L_B is a constant regardless of υ_d, the force-accelerated spontaneous breaking (FA) regime, where L_B monotonically diminishes with decreasing υ_d, and the self-breaking (SB) regime, where L_B approaches zero whereas τ_B saturates.

Constant $L_B \sim 0.3$ nm in the FB regime suggests preferential breaking of the single atom chains at a specific length. The breaking mechanism of Au SACs was previously investigated in detail at 4.2 K.[19] It was elucidated that mechanical stretching elongates the Au−Au interatomic distance in the monatomic chain. When the bond length is extended to approximately 0.25 nm, the stored elastic energy relaxes via atomic rearrangements through incorporation of an additional atom into the chain. The lengthening process repeats until the force approaches the tensile limit of ∼1.5 nN. Experimentally, multiple peaks were observed in the length histogram at integral multiples of the critical bond length ∼0.25 nm.[19] In fact, we obtained a similar peak structure with an inter-peak period of about 0.20 nm when representing $P(\tau)$ against υ_d in a linear scale (Figure 4a). The analogy shows that the mechanical loading is the dominant contact rupture mechanism at the high stretching rates. Observations of parity oscillations further corroborate the mechanical force origin of the junction breaking.[20] Regular conductance oscillations are occasionally observed at $\sim 1G_0$ (Figure 4, panels b and c). The half period of the fluctuations possess relatively narrow distributions of $t_p = 25 \pm 2$ ms and 46 ± 10 ms at $\upsilon_d = 8$ and 4 nm/s, respectively. The chain length period calculated from t_p well-

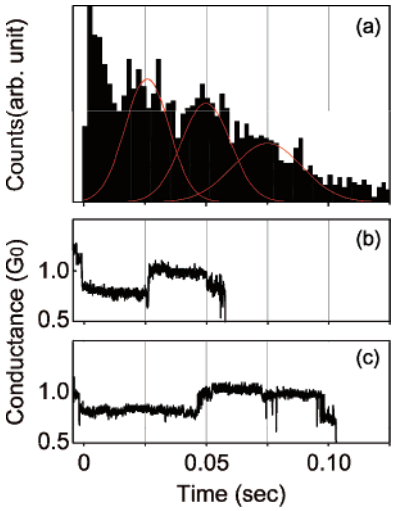

Figure 4. (a) $P(\tau)-\tau$ histogram at 8 nm/s revealing equally spaced peaks at an integral multiple of about 0.02 s. The red curves are a Gaussian fit. (b) Examples of parity oscillations observed at 8 and (c) 4 nm/s.

coincides with the estimated Au−Au bond length of ∼0.2 nm within 1% ($\upsilon_d = 8$ nm/s) and 9% ($\upsilon_d = 4$ nm/s) of deviation. The correspondence relation between t_p and the interatomic distance accords with the characteristics of the even−odd conductance modulations observed at low temperatures.[20] That t_p is inversely proportional to υ_d unambiguously indicates that the mechanical loading prevails in the junction breaking under the high stretching rate conditions.

At the other extreme, L_B approaches zero and simultaneously τ_B levels off in SB regime. The extremely low loading rate at $\upsilon_d \leq 0.008$ nm/s no longer seems adequate for causing detectable effects on the contact life time and, hence, negligible contributions of mechanical stretching on the contact breakdown. The junction breakdown characteristics under the low-υ_d conditions are of particular interest as the no-tension circumstance is ideal for inspecting the self-breaking mechanism. It is noticeable that, while persisting a single peak pattern, the low-υ_d life time distribution significantly expands toward the high-τ_c range, in contrast to an overall trend that $P(\tau)$ rapidly declines after showing a sharp peak at τ_B. In the broad lifetime distribution in the SB regime, it seems inexplicable that some junctions are capable of substantial elongation. For instance, the SACs with $\tau > 200$ s at the stretching rates of 0.008 nm/s logically evolve into a chain of an extraordinary length exceeding 1.5 nm. We speculate that sufficient contact structure relaxations take place by atomic rearrangements at the banks of the chains under the low displacement speeds. Indeed, the stretching rate of 0.008 nm/s is already comparable to the surface diffusion velocity of gold atoms, which is measured to be 0.02−0.003 nm/s at room temperatures.[21,22] As a result, the contacts are able to fully self-compensate for the mechanically induced strains. Thus, the junction breakdown mechanism in the SB regime is thermoactivated self-breaking under a completely stress-free condition. The life time distribution under the load-free conditions originates from the intrinsic variation of E_B. Assuming $F = 0$ enables back calculation of the energy barrier. From $P(\tau)$ obtained at 0.0008

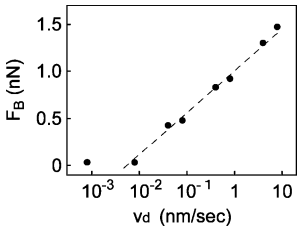

Figure 5. Breakdown force plotted as a function of log(v_d). The broken line is a linear fit to the plot. The force decreases logarithmically with the stretching rate.

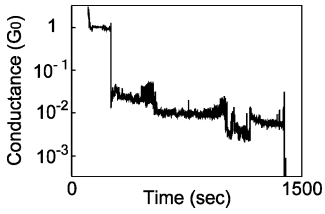

Figure 6. Typical conductance trace of Au/benzenedithiol/Au junctions obtained at 0.0008 nm/s. The clear conductance step at $\sim 0.01 G_0$ signifies formation of a benzenedithiol single molecule contacts.[30] A single molecule junction is sustained for about 19 min in this trial.

nm/s, eq 1 yields a relatively narrow distribution of E_B centered at ~0.8 eV with a half width of ~0.1 eV. This E_B is in quantitative accordance with the theoretical estimation.[16]

As we have seen, the stress accumulation effectively reduces the energy barrier for thermally activated contact breakdown. If the loading rate is sufficiently high, the energy barrier would decrease to zero rapidly enough for thermal fluctuations to demonstrate any notable roles, and the contacts tend to break at a specific length irrespective of v_d. On the contrary, when the stretching rate is made comparable or slower than the atomic diffusion velocity, the external tensile force completely relaxes by virtue of efficient atomic rearrangements in the vicinity of the contacts. The junctions would then exhibit the thermally activated self-breaking. In between the two distinct realms lies the force-accelerated spontaneous breakdown regime where the contacts fracture at an appropriate level of external force at which the thermally activated dissociation is most likely to occur. The breakdown force, F_B, is estimated from τ_B. The energy barrier is ~0.8 eV, the natural life time of the contacts obtained at the self-breaking regime. Based on eq 1, $\tau_B \sim 0.04$ s at $v_d = 8$ nm/s gives $\alpha F_B \sim 0.15$ eV. As the force breaking of the contacts typically occurs at $F_B \sim 1.5$ nN,[24,25] the ultimate tensile strength of the contacts, $\alpha \sim 0.1$ eV/nN. The calculated F_B scales linearly with log(v_d) as shown in Figure 5. Meanwhile, analogous to F_B, the breaking length L_B demonstrates linear-log dependence with v_d as depicted in Figure 3. Therefore, $F_B = k_f L_B$ with a force constant $k_f \sim 3.8$ N/m. The obtained stiffness of Au single atom chains is quantitatively consistent with the results of AFM-based force measurements,[24−26] the agreement of which constitutes verification of validity of the $L_B - v_d$ measurement as a practical tool to probe force exerted on atomic-scale systems.

The linear proportionality between F_B and L_B defines a loading rate $r_d = k_f v_d$, and hence, $F_B \propto \log(r_d)$. It is noted that the linear $F_B - \log(r_d)$ dependence is well-established in biological systems[27] and has already been observed for Au single atom contacts in recent SPM break junction experiments.[28] Nevertheless, there are several disagreements in the $L_B - \log(v_d)$ characteristics; for example, the second plateau at $L_B \sim 0.1$ nm was observed in ref 28, whereas L_B monotonically decreased to 0 in the present study. The inconsistency probably stems from the difference in the test environments, i.e., vacuum versus solution. It is also suspected that a finite mechanical vibration in the SPM system limited the contact lifetime at the slow stretching speeds, as it is indicated that mere angstrom-scale fluctuations can cause significant degradation of the contact stability. However, there is no clear-cut evidence at this time to have a conclusive argument on the experimental discrepancy.

The finding that forming and holding stable Au single atom contacts for a prolonged time at a room-temperature necessitates fine control of the junction displacements with precision better than picometer-order has an important implication for the study of electron transport in single molecule junctions. The breakdown of metal/molecule/metal junctions with the extensively employed Au−S system is known to occur at Au−Au bonds near the metal−molecule interface.[29] The nature of the molecular junction stability is, therefore, expected to share many aspects in common with that of Au atom-sized contacts. Indeed, recent experiments on breakdown mechanisms of Au/alkanedithiol/Au junctions revealed that they undergo thermally activated fracture in qualitatively the same manner as that of metal junctions.[28] The present results thus suggest the critical importance of employing experimental systems with subpicometer mechanical stability for performing reliable electrical property measurements of single molecules. In our preliminary experiments on the Au/benzenedithiol/Au system, actually, it is observed that the single molecule junctions can be held for more than 10 min at the low displacement rates with our nanofabricated MCBJs (Figure 6), the capability of which provides a practical experimental platform to explore the charge transport mechanism in single molecules.

In summary, the self-breaking mechanism of Au junctions is explored at room temperature by investigating the lifetime of the single atom contacts at various stretching rate conditions. A profound effect of external forces on stability of the break junctions was revealed. The breakdown force was observed to decrease logarithmically with the contact stretching rate. Only at an extremely low stretching rate of 0.0008 nm/s did the junctions demonstrate a static thermo-activated breakdown in the self-breaking processes. It was elucidated that the contacts self-recover the external strain by contact structure relaxation. The present results have significance for building reliable single molecule devices.

References

(1) Xu, B.; Tao, N. J. *Science* **2003**, *301*, 1221.
(2) Smit, R. H. M.; Noat, Y.; Untiedt, C.; Lang, N. D.; van Hemert, M. C.; van Ruitenbeek, J. M. *Nature* **2002**, *419*, 906.
(3) Blum, A. S.; Kushmerick, J. G.; Long, D. P.; Patterson, C. H.; Yang, J. C.; Henderson, J. C.; Yao, Y.; Tour, J. M.; Shashidhar, R.; Ratna, B. R. *Nature Mat.* **2005**, *4*, 167.

(4) Kubatkin, S.; Danilov, A.; Hjort, M.; Cornil, J.; Bredas, J.-C.; Stuhr-Hansen, N. Hedegard, P.; Bjomholm, T. *Nature* **2003**, *425*, 698.
(5) Park, H.; Lim, A. K. L.; Alivisatos, P.; Park, J.; McEuen, P. L. *Appl. Phys. Lett.* **1999**, *75*, 301.
(6) Poot, M.; Osorio, E.; O'Neill, K.; Thijssen, J. M.; Vanmaekelbergh, D.; van Walree, C. A.; Jenneskens, L. W.; van der Zant, H. S. J. *Nano Lett.* **2006**, *6*, 1031.
(7) Trouwborst, M. L.; van der Molen, S. J.; van Wees, B. J. *J. Appl. Phys.* **2006**, *99*, 114316.
(8) Taychatanapat, T.; Bolotin, K. I.; Kuemmeth, F.; Ralph, D. C. *Nano Lett.* **2007**, *7*, 652.
(9) Houck, A. A.; Labaziewicz, J.; Chan, E. K.; Folk, J. A.; Chuang, I. L. *Nano Lett.* **2005**, *5*, 1685.
(10) Sordan, R.; Balasubramanian, K.; Burghard, M.; Kern, K. *Appl. Phys. Lett.* **2005**, *84*, 013106.
(11) O'Neill, K.; Osorio, E. A.; van der Zant, H. S. *Appl. Phys. Lett.* **2007**, *90*, 133109.
(12) Osorio, E. A.; O'Neill, K.; Wegewijs, M.; Stuhr-Hansen, N.; Paaske, J.; Bjornholm, T.; van der Zant, H. S. J. *Nano Lett.* **2007**, *7*, 3336.
(13) van Ruitenbeek, J. M.; Alvarez, A.; Pineyro, I.; Grahmann, C.; Joyez, P.; Devoret, M. H.; Esteve, D.; Urbina, C. *Rev. Sci. Instrum.* **1996**, *67*, 108.
(14) Vrouwe, S. A. G., van der Giessen, E.; van der Molen, S. J.; Trouwborst, M. L.; van Wees, B. J. *Phys. Rev. B* **2005**, *71*, 035313.
(15) Lortscher, E.; Weber, H. B.; Riel, H. *Phys. Rev. Lett.* **2007**, *98*, 176807.
(16) Todorov, T. N.; Hoekstra, J.; Sutton, A. P. *Phys. Rev. Lett.* **2001**, *86*, 3606.
(17) Chen, Y.-C.; Zwolak, M.; Di Ventra, M. *Nano Lett.* **2003**, *3*, 1691.
(18) Suzuki, R.; Tsutsui, M.; Miura, D.; Kurokawa, S.; Sakai, A. *Jpn. J. Appl. Phys.* **2007**, *46*, 3694.
(19) Untiedt, C.; Yanson, A. I.; Grande, R.; Rubio-Bollinger, G.; Agrait, N.; Vieira, S.; van Ruitenbeek, J. M. *Phys. Rev. B* **2002**, *66*, 085418.
(20) Smit, R. H. M.; Untiedt, C.; Rubio-Bollinger, G.; Segers, R. C.; van Ruitenbeek, J. M. *Phys. Rev. Lett.* **2003**, *91*, 076805.
(21) Roberts, C. J.; Hoffmann-Millack, B.; Steer, W. S. *J. Vac. Sci. Technol. B* **1990**, *9*, 841.
(22) We note that bias-induced local heating plays a minimal role on the atomic diffusion rates for $T_{\mathrm{eff}} \sim T_0 = 293$ K from eq 2 since $T_{\mathrm{V}} \ll T_0$ at 0.1 V, due to efficient lattice thermal cooling of the contacts.[23]
(23) Tsutsui, M.; Kurokawa, S.; Sakai, A. *Nanotechnology* **2006**, *17*, 5334.
(24) Rubio-Bollinger, G.; Agrait, N.; Vieira, S. *Phys. Rev. Lett.* **1996**, *76*, 2302.
(25) Rubio-Bollinger, G.; Bahn, S. R.; Agrait, N.; Jacobsen, K. W.; Vieira, S. *Phys. Rev. Lett.* **2001**, *87*, 026101.
(26) Jarvis, S. P.; Lantz, M. A.; Ogiso, H.; Tokumoto, H.; Durig, U. *Appl. Phys. Lett.* **1999**, *75*, 3132.
(27) Evans, E. *Annu. Rev. Biophys. Biomol. Struct.* **2001**, *30*, 105.
(28) Huang, Z.; Chen, F.; Bennett, P. A.; Tao, N. J. *J. Am. Chem. Soc.* **2007**, *129*, 13225.
(29) Xu, B.; Xiao, X.; Tao, N. J. *J. Am. Chem. Soc.* **2003**, *125*, 16164.
(30) Xiao, X.; Xu, B.; Tao, N. J. *Nano Lett.* **2004**, *4*, 267.

NL073003J